

National Center of Competence in Research Quantum Science and Technology, the Army Research Office (ARO) Multidisciplinary University Research Initiative (MURI) grant no. W911NF11-1-0268, ARO grant no. W911NF-12-1-0523, the Lockheed Martin Corporation, and Microsoft Research. Simulations were performed on clusters at Microsoft Research and ETH Zurich on supercomputers of the Swiss Center for Scientific Computing.

We acknowledge hospitality of the Aspen Center for Physics, supported by NSF grant PHY-1066293.

SUPPLEMENTARY MATERIALS

www.sciencemag.org/content/345/6195/420/DC1
Supplementary Text
Figs. S1 to S10

Tables S1 and S2
References (31–37)

17 February 2014; accepted 10 June 2014
Published online 19 June 2014;
10.1126/science.1252319

QUANTUM METROLOGY

Fisher information and entanglement of non-Gaussian spin states

Helmut Strobel,^{1*} Wolfgang Muessel,¹ Daniel Linnemann,¹ Tilman Zibold,¹ David B. Hume,¹ Luca Pezzè,² Augusto Smerzi,² Markus K. Oberthaler¹

Entanglement is the key quantum resource for improving measurement sensitivity beyond classical limits. However, the production of entanglement in mesoscopic atomic systems has been limited to squeezed states, described by Gaussian statistics. Here, we report on the creation and characterization of non-Gaussian many-body entangled states. We develop a general method to extract the Fisher information, which reveals that the quantum dynamics of a classically unstable system creates quantum states that are not spin squeezed but nevertheless entangled. The extracted Fisher information quantifies metrologically useful entanglement, which we confirm by Bayesian phase estimation with sub-shot-noise sensitivity. These methods are scalable to large particle numbers and applicable directly to other quantum systems.

Multiparticle entangled states are the key ingredients for advanced quantum technologies (1). Various types have been achieved in experimental settings ranging from ion traps (2), photonic systems (3), and solid state circuits (4) to Bose-Einstein condensates. For the latter, squeezed states (5, 6) have been generated (7–12), and a rich class of entangled non-Gaussian states is predicted to be obtainable (13), including maximally entangled Schrödinger cat states (14, 15). The production of these fragile states in large systems remains a challenge, and efficient methods for characterization are necessary because full state reconstruction becomes intractable. Here, we generate a class of non-Gaussian many-particle entangled states and reveal their quantum properties by studying the distinguishability of experimental probability distributions.

A measure of the distinguishability with respect to small phase changes of the state is provided by the Fisher information F (16). It is related to the highest attainable interferometric phase sensitivity by the Cramer-Rao bound $\Delta\theta_{\text{CR}} = 1/\sqrt{F}$ (17). This limit follows from general statistical arguments for a measurement device with fluctuating output (18). The Fisher information is limited by quantum fluctuations of the input state as

well as the performance of the device. Even in the absence of technical noise, the Fisher information of a classical input state is $F \leq N$ because

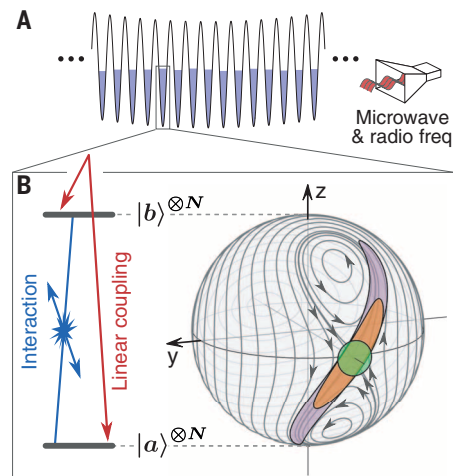


Fig. 1. Preparation and detection of non-Gaussian entangled states. (A) Array of Bose-Einstein condensates in an optical lattice potential addressed by microwave and radio frequency fields. (B) The interplay of nonlinear interaction (blue) and weak Rabi coupling (red) between the internal states $|a\rangle$ and $|b\rangle$ results in an unstable fixed point in the classical phase space. The state of the system is visualized on a generalized Bloch sphere with radius $J = N/2$. Gray lines indicate trajectories of the mean-field equations of motion (18). The initial coherent spin state (green) ideally evolves into a squeezed state (orange) followed by non-Gaussian states at later evolution times (violet). Edges of shaded areas are contours of the Husimi distribution for $N = 380$ at $1/e^2$ of its maximum. (C) Experimental absorption picture showing the site- and state-resolved optical lattice after a Stern-Gerlach separation. Shaded boxes indicate the sites with a total atom number in the range of 380 ± 15 , which are selected for further analysis. (D) Example histograms of the imbalance $z = 2J_z/N$ after nonlinear evolution of 25 ms and final rotation (angles indicated in the graphs) compared with the ideal coherent spin state of identical N (green Gaussian).

¹Kirchhoff-Institut für Physik, Universität Heidelberg, Im Neuenheimer Feld 227, 69120 Heidelberg, Germany. ²QSTAR (Quantum Science and Technology in Arcetri), INO-CNR (Istituto Nazionale di Ottica–Consiglio Nazionale delle Ricerche), and LENS (European Laboratory for Nonlinear Spectroscopy), Largo Enrico Fermi 2, 50125 Firenze, Italy.
*Corresponding author. E-mail: fisherinformation@matterwave.de

of the intrinsic granularity of N independent particles, which translates into the shot-noise limit $\Delta\theta \geq 1/\sqrt{N}$ for phase estimation. This classical bound can be surpassed with a reduction of the input fluctuations by introducing entanglement between the N particles (5). These states, known as squeezed states, are fully characterized by mean and variance of the observable and already used in precision measurements (19–21). In contrast, non-Gaussian quantum states can have increased fluctuations of the observable but nevertheless allow surpassing shot-noise limited performance. A textbook example is the Schrödinger cat state characterized by macroscopic fluctuations but achieving the best interferometric performance allowed by quantum mechanics, that is, at the fundamental Heisenberg limit $F = N^2$ (22). In general, the class of states that are entangled and useful for sub-shot-noise phase estimation is identified by the Fisher information criterion $F > N$ (13). Exploiting these resources requires probabilistic methods for phase estimation, such as maximum likelihood or Bayesian analysis (23), which go beyond standard evaluation of averages.

A paradigm physical process that exhibits the transition from Gaussian to non-Gaussian states is the time evolution of a quantum state initially prepared at an unstable classical fixed point. Our experimental system is an array of interacting binary Bose-Einstein condensates of ^{87}Rb with additional linear coupling of the two internal states (Fig. 1, A and B), which allows for the controlled realization of such unstable fixed point dynamics (24). The linear coupling, realized with microwave and radio frequency magnetic fields, also permits precise rotations for initial state preparation and final state manipulation before readout (Fig. 1, B and D). For a coherent state initially centered on the unstable fixed point, the quantum dynamics leads to spin squeezed states for short evolution times; subsequently, the squeezed states transform into non-Gaussian states on an experimentally feasible time scale (14) (Fig. 1B).

For the characterization of non-Gaussian states, higher moments, or even the full probability distributions, have to be accessed experimentally. For this, the setup (8) has been extended to realize up to 35 individual condensates in a single experiment, which permits the acquisition of sufficient statistics in a narrow window of ± 15 for the final atom number. The populations of the atomic states $|a\rangle = |F = 1, m_F = 1\rangle$ and $|b\rangle = |F = 2, m_F = -1\rangle$ are destructively detected for each individual condensate by state-selective absorption imaging with high spatial resolution (Fig. 1C) (25). By repeating the experiment (typically many thousands of times), we measure the experimental probability distributions of the population imbalance $z = (N_b - N_a)/N$ along defined directions by applying the corresponding spin rotation before detection. The analysis window for $N = N_b + N_a$ is adjusted according to the independently determined time scale of atom loss (18) to follow the time evolution start-

ing with $\langle N \rangle = 470$. Figure 1D shows examples of observed distributions for two different orientations and an evolution time of 25 ms; the distributions are consistent with the theoretically expected structure of the state (Fig. 1B).

Detailed insight can be gained by repeating this measurement for various angles (here in steps of 10°) allowing for the maximum-likelihood reconstruction of the density matrix in the symmetric subspace (18). The tomography results obtained from 32,500 experimental realizations (Fig. 2A) confirm qualitatively the expected behavior; at short evolution times, the state has a squeezed shape, whereas at later times the characteristic bending dynamics appears as expected from the presence of the two stable fixed points above and below the equator.

Analyzing the variance of z for the same data as a function of the tomography angle (Fig. 2B) shows that the time evolution leads to suppressed fluctuations at 15 ms. Extracting the spin squeezing parameter ξ^2 (18), we find that the minimum is $\xi_{\min}^2 = -4.5 \pm 0.2$ dB below the standard quantum limit, which demonstrates entanglement (5). For all results reported here, the photon shot noise of the absorption imaging of ± 4 atoms is not subtracted. For longer time evolution, the bending dynamics leads to increased fluctuations in all directions, that is, tomography angles. After 25 ms, spin squeezing is lost, and we find that $\xi_{\min}^2 = -0.2 \pm 0.3$ dB. However, experimental extraction of the Fisher information (detailed below, Fig. 2C) reveals that useful entanglement is still present although spin squeezing is vanishing, that is, $F/N \geq 1/\xi^2$ (13). At 26 ms, spin squeezing is completely lost, whereas the Fisher information still indicates the presence of quantum resources ($F/N > 1$). In the Gaussian regime up to 23 ms, we observe that Fisher information and the inverse spin

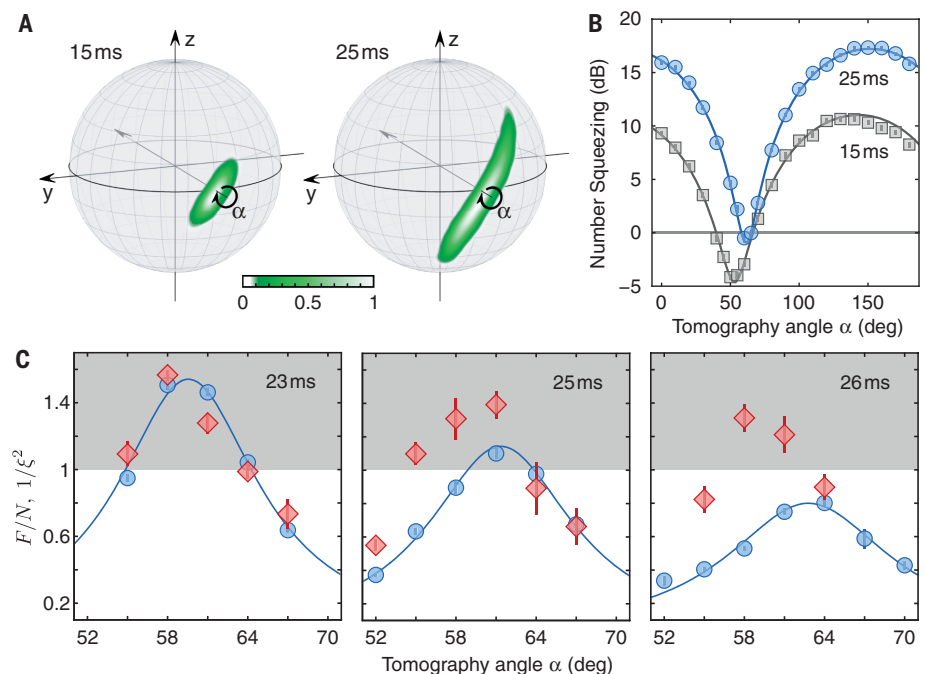
squeezing agree as expected, $F/N \approx 1/\xi^2$, because these states are fully characterized by their variance.

Our method for extraction of the Fisher information circumvents the experimentally intractable full reconstruction of the density matrix and has its basis in a specific set of experimental probability distributions $P_z(\theta)$ after small rotations θ of the quantum state. In Fig. 3A, we show distributions for the state created at 26 ms and the optimal tomography angle of 58° (Fig. 2C) after small rotations about the y axis (Fig. 3C, inset). The distributions feature a pronounced peak and long tails characteristic for the bent state. The main effect of the small rotation is a continuous shift of the distribution toward increasing imbalance for larger angles θ .

The analysis for extraction of the Fisher information builds on the statistical distance (26, 27) of these distribution functions. We use a Euclidean distance in the space of probability amplitudes $\sqrt{P_z}$ known as Hellinger distance (18), defined as $d_H^2(\theta) = \frac{1}{2} \sum_z [\sqrt{P_z(\theta)} - \sqrt{P_z(0)}]^2$, where $P_z(\theta)$ is the experimental probability distribution at angle θ . Figure 3C shows $d_H^2(\theta)$ as a function of θ for three different evolution times and the respective optimal tomography angles. A resampling method (18) is used to extract error bars and reduce the statistical bias. The observed quadratic behavior is expected from the Taylor expansion $d_H^2(\theta) = (F/8)\theta^2 + \mathcal{O}(\theta^3)$ (eq. S11), which reveals the close connection between Hellinger distance and Fisher information; this relationship is used to extract F from the curvature of $d_H^2(\theta)$. The gray shaded area in Fig. 3C indicates the region that is not accessible to separable states; for them, the Fisher information is limited to $F/N \leq 1$, resulting in a d_H^2 curvature smaller than $N/8$. For the initially prepared state, we found a Fisher information of

Fig. 2. Entangled state characterization.

(A) Tomographic reconstruction of the experimental state after evolution times of 15 and 25 ms. The Husimi projections [scaled amplitude is brightness-coded (18)] confirm the creation of an elongated state and the subsequent distortion of the Gaussian shape. (B) A variance analysis of the particle number difference reveals maximum spin squeezing of -4.5 ± 0.2 dB for 15 ms and -0.2 ± 0.3 dB for 25 ms. (C) Comparison of the normalized Fisher information F/N (red diamonds) for $N = 380 \pm 15$ atoms and the inverted spin squeezing factor $1/\xi^2$ (blue circles). The gray shaded areas are only accessible for nonseparable (entangled) states. For 26 ms, spin squeezing cannot identify the entanglement that is detected by the Fisher information. Lines are sinusoidal fits; error bars of the Fisher information represent the 68% confidence interval of the Hellinger distance method.



$F/N = 0.91 \pm 0.04 < 1$, which is expected for a separable state. All given error margins are ± 1 SE. For a subsequent evolution of 26 ms, the measured Hellinger distances lie in the regime of nonseparability. This reveals entanglement in a regime where no spin squeezing is present. For the intermediate evolution time of 15 ms, we extract a Fisher information $F/N = 2.2 \pm 0.2$, which confirms entanglement in the Gaussian spin squeezed state. For obtaining the experimental points in Fig. 2C, this procedure is performed at a given evolution time for different tomography angles. The reported values for the Fisher information are limited by experimental imperfections, detection noise, and atom loss, which especially affect the fragile non-Gaussian states. For the ideal time evolution, monotonically increasing Fisher information is expected, whereas the available spin squeezing is limited to $1/\xi^2 \approx 18$ (-12.6 dB). The ideal theoretical model prediction is $F/N \approx 90$ (-19.5 dB) for the evolution time when spin squeezing vanishes (18).

There is a direct connection between Fisher information and sensitivity in parameter estimation. In an interferometric context, high sensitivity, indicated by a large value of F , means fast change of the output distribution with the phase θ , that is, high statistical speed $\partial d_H/\partial\theta = \sqrt{F/8}$ with respect to the parameter change. For the quantum state at 25 ms, the enhanced Fisher information reveals quantum resources beyond the standard quantum limit in a range of tomography angles. In Fig. 4A, we show explicitly through an analysis of mean and variance that averaging of the observable z does not surpass shot-noise limited performance for rotations about the y axis [corresponding, for example, to a phase shift inside a Ramsey interferometer (18)].

However, the resource can be harnessed with model-independent Bayesian estimation by using the experimental probability distributions $P_z(\theta)$. For this, we use an independent data set taken with the setting ($\alpha = 58^\circ, \theta = \theta_0 = 0^\circ$) and 25 ms of evolution time, which we divide into sequences $\{z_1, \dots, z_m\}$ each containing m realizations. To obtain realistic measurement conditions, we discard the previous knowledge on the true value of the phase θ_0 [Bayesian estimation with flat prior (18)]. For each distribution $P_z(\theta_i)$, we calculate the likelihood $\mathcal{L}(\theta_i) = \prod_{j=1}^m P_{z_j}(\theta_i)$, which corresponds to the conditional probability to obtain the sequence $\{z_1, \dots, z_m\}$ if the phase setting had been θ_i . For sufficiently large m , we expect a Gaussian distribution $\mathcal{L}(\theta) \propto \exp[-(\theta - \theta_c)^2/2\sigma^2]$ centered at θ_c with the Bayesian phase uncertainty σ (18). Thus, σ can be extracted from a quadratic fit to $\log \mathcal{L}(\theta)$ (Fig. 4B, inset). We find a fast convergence of σ^2 to the expected value $1/mF$ (Cramer-Rao bound for m measurements) already for $m \geq 2$ (Fig. 4B). This explicitly shows phase uncertainty below the standard quantum limit in agreement with the Fisher information obtained from the Hellinger distance method described above.

Fisher information serves to verify entanglement in the absence of spin squeezing and quantifies

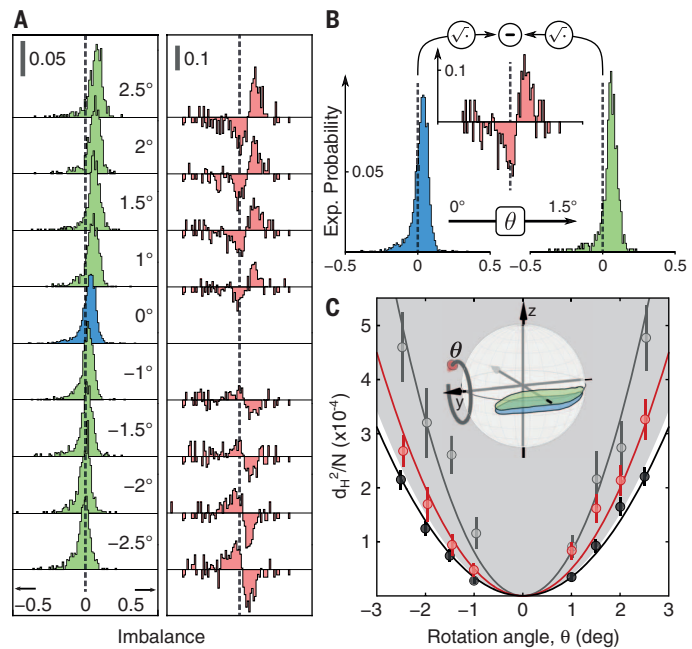


Fig. 3. Experimental extraction of the Fisher information. (A) Examples of experimental histograms of z (left) after 26 ms of evolution time obtained for the tomography angle $\alpha = 58^\circ$ and additional small rotation angles θ about the y axis [see inset of (C)]. The blue histogram is used as a reference for the following analysis. The right column shows the square-root differences between the respective histogram and the reference [see (B)]. Gray bars indicate the vertical scales [see axes in (B)]. (B) Extraction of the squared Hellinger distance (example of $\theta = 1.5^\circ$). Probability amplitudes $\sqrt{P_z}$ for $\theta = 1.5^\circ$ (green) and $\theta = 0^\circ$ (blue) are subtracted for each bin (red), and these differences are squared and summed to obtain the squared Hellinger distance. (C) Squared Hellinger distance for three evolution times. A reference measurement (black) with the initial coherent spin state (0 ms evolution) lies slightly outside the nonclassical region (gray shaded area). The spin squeezed state (gray, 15-ms evolution) surpasses the classical limit. After 26 ms [red points, histograms shown in (A)], the state has a non-Gaussian shape, is not spin squeezed, but still performs beyond the standard quantum limit. Error bars indicate the statistical 68% confidence interval obtained by a resampling procedure (18). The curvature of the quadratic fit is proportional to F/N .

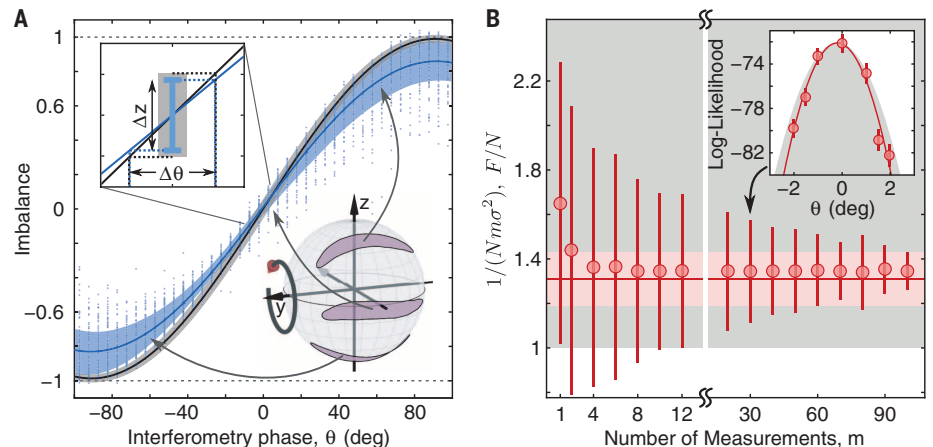


Fig. 4. Quantum enhanced phase sensitivity in the absence of spin squeezing. (A) A rotation on the Bloch sphere by the angle θ (right inset) is formally equivalent to the action of a Ramsey interferometer with relative phase shift θ (fig. S5). Interference fringe of z (blue line with 68% confidence interval) with the state after 25-ms evolution and subsequent tomography rotation of 61° ; reference measurement with a coherent spin state (black line with gray confidence region). The phase sensitivity $\Delta\theta$ deduced from standard error propagation via the slope of the interferometer fringe (left inset) does not surpass the standard quantum limit. (B) Bayesian analysis with the tomography angle for maximal Fisher information (58°). For each sequence of length m , a quadratic fit to $\log \mathcal{L}$ is used to extract the Gaussian variance σ^2 of \mathcal{L} (inset), which corresponds to the phase sensitivity. The value of $1/(Nm\sigma^2)$ as a function of m shows fast convergence to the extracted F/N obtained with the Hellinger distance method (red line with 68% confidence region). The error bars indicate the standard deviation of a single sequence. Gray shaded regions are only accessible with entanglement in the system.

the quantum resource for improved phase estimation. The presented method does not depend on the special shape of the probability distributions and is not limited to small particle numbers. It is therefore broadly applicable to the efficient characterization of highly entangled states, relevant for further improvement of atom interferometers (8, 11, 12, 19, 20, 28–30) toward the ultimate Heisenberg limit (22). More generally, it can be applied to any phenomenon characterizable by the distinguishability of quantum states, as in quantum phase transitions (31), quantum Zeno dynamics (32), and quantum information protocols (1).

REFERENCES AND NOTES

- M. A. Nielsen, I. L. Chuang, *Quantum Computation and Quantum Information* (Cambridge Univ. Press, Cambridge, 2000).
- R. Blatt, D. Wineland, *Nature* **453**, 1008–1015 (2008).
- J.-W. Pan *et al.*, *Rev. Mod. Phys.* **84**, 777–838 (2012).
- B. Vlastakis *et al.*, *Science* **342**, 607–610 (2013).
- A. Sørensen, L.-M. Duan, J. I. Cirac, P. Zoller, *Nature* **409**, 63–66 (2001).
- D. J. Wineland, J. J. Bollinger, W. M. Itano, D. J. Heinzen, *Phys. Rev. A* **50**, 67–88 (1994).
- J. Estève, C. Gross, A. Weller, S. Giovanazzi, M. K. Oberthaler, *Nature* **455**, 1216–1219 (2008).
- C. Gross, T. Zibold, E. Nicklas, J. Estève, M. K. Oberthaler, *Nature* **464**, 1165–1169 (2010).
- M. F. Riedel *et al.*, *Nature* **464**, 1170–1173 (2010).
- C. D. Hamley, C. S. Gerving, T. M. Hoang, E. M. Bookjans, M. S. Chapman, *Nat. Phys.* **8**, 305–308 (2012).
- T. Berrada *et al.*, *Nat. Commun.* **4**, 2077 (2013).
- B. Lücke *et al.*, *Science* **334**, 773–776 (2011).
- L. Pezzé, A. Smerzi, *Phys. Rev. Lett.* **102**, 100401 (2009).
- A. Micheli, D. Jaksch, J. I. Cirac, P. Zoller, *Phys. Rev. A* **67**, 013607 (2003).
- J. I. Cirac, M. Lewenstein, K. Mølmer, P. Zoller, *Phys. Rev. A* **57**, 1208–1218 (1998).
- R. A. Fisher, *Proc. Camb. Philos. Soc.* **22**, 700–725 (1925).
- C. W. Helstrom, *Quantum Detection and Estimation Theory* (Academic Press, New York, 1976).
- Materials and methods are available as supplementary materials on Science Online.
- R. J. Sewell *et al.*, *Phys. Rev. Lett.* **109**, 253605 (2012).
- C. F. Ockeloen, R. Schmied, M. F. Riedel, P. Treutlein, *Phys. Rev. Lett.* **111**, 143001 (2013).
- R. Schnabel, N. Mavalvala, D. E. McClelland, P. K. Lam, *Nat. Commun.* **1**, 121 (2010).
- V. Giovannetti, S. Lloyd, L. Maccone, *Phys. Rev. Lett.* **96**, 010401 (2006).
- R. Krschek *et al.*, *Phys. Rev. Lett.* **107**, 080504 (2011).
- T. Zibold, E. Nicklas, C. Gross, M. K. Oberthaler, *Phys. Rev. Lett.* **105**, 204101 (2010).
- W. Muessel *et al.*, *Appl. Phys. B* **113**, 69–73 (2013).
- W. K. Wootters, *Phys. Rev. D* **23**, 357–362 (1981).
- S. L. Braunstein, C. M. Caves, *Phys. Rev. Lett.* **72**, 3439–3443 (1994).
- J. Appel *et al.*, *Proc. Natl. Acad. Sci. U.S.A.* **106**, 10960–10965 (2009).
- I. D. Leroux, M. H. Schleier-Smith, V. Vuletić, *Phys. Rev. Lett.* **104**, 250801 (2010).
- Z. Chen, J. G. Bohnet, S. R. Sankar, J. Dai, J. K. Thompson, *Phys. Rev. Lett.* **106**, 133601 (2011).
- P. Zanardi, M. G. A. Paris, L. Campos Venuti, *Phys. Rev. A* **78**, 042105 (2008).
- A. Smerzi, *Phys. Rev. Lett.* **109**, 150410 (2012).

ACKNOWLEDGMENTS

We thank J. Tomkovič, E. Nicklas, and I. Stroescu for technical help and discussions. This work was supported by the Forschergruppe FOR760, the Deutsche Forschungsgemeinschaft, the Heidelberg Center for Quantum Dynamics, and the European Commission small or medium-scale focused research project QIBEC (Quantum Interferometry with Bose-Einstein condensates, contract no. 284584). W.M. acknowledges support by the Studienstiftung des

deutschen Volkes. D.B.H. acknowledges support from the Alexander von Humboldt Foundation. L.P. acknowledges financial support by Ministero dell'Istruzione, dell'Università e della Ricerca through Fondo per gli Investimenti della Ricerca di Base project no. RBFR08HO58. QSTAR is the Max Planck Institute of Quantum Optics, LENS, Istituto Italiano di Tecnologia, Università degli Studi di Firenze Joint Center for Quantum Science and Technology in Arcetri.

SUPPLEMENTARY MATERIALS

www.sciencemag.org/content/345/6195/424/suppl/DC1
Materials and Methods
Figs. S1 to S5
References (33–38)

24 December 2013; accepted 3 June 2014
10.1126/science.1250147

METAMATERIALS

Invisibility cloaking in a diffusive light scattering medium

Robert Schittny,^{1,2} Muamer Kadic,^{1,3} Tiemo Bückmann,^{1,2} Martin Wegener^{1,2,3*}

In vacuum, air, and other surroundings that support ballistic light propagation according to Maxwell's equations, invisibility cloaks that are macroscopic, three-dimensional, broadband, passive, and that work for all directions and polarizations of light are not consistent with the laws of physics. We show that the situation is different for surroundings leading to multiple light scattering, according to Fick's diffusion equation. We have fabricated cylindrical and spherical invisibility cloaks made of thin shells of polydimethylsiloxane doped with melamine-resin microparticles. The shells surround a diffusively reflecting hollow core, in which arbitrary objects can be hidden. We find good cloaking performance in a water-based diffusive surrounding throughout the entire visible spectrum and for all illumination conditions and incident polarizations of light.

With an invisibility cloak (1–5), light is guided in a detour around an object to be hidden so that it emerges behind as though no object was there. Ideally, this concerns the direction, amplitude, and timing of light. In vacuum (or air) and for macroscopic objects much larger than the wavelength of light, this geometrical detour means that the local velocity of light must exceed the vacuum speed of light somewhere. For broadband operation—in the absence of wavelength dependence—the phase velocity of light equals its energy velocity. Furthermore, according to the theory of relativity, energy and mass are equivalent, and transport of mass faster than the vacuum speed of light is not possible. Thus, ideal passive broadband invisibility cloaking of macroscopic objects in vacuum (or air) is not consistent (4, 5) with relativity and Maxwell's equations of electromagnetism.

Nevertheless, inspired by transformation optics (1–3) based on Maxwell's equations, many interesting cloaking experiments have been performed (6–12). All of these cloaks, however, are either narrow in bandwidth or not macroscopic, do not properly recover the time-of-flight (or phase), work only for restricted polarizations or directions of light, or exhibit combinations of these limitations.

In many practical instances, light does not propagate ballistically—it cannot be described adequately by the macroscopic Maxwell equations for continua. For example, in clouds, fog, milk,

frosted glass, or in other systems containing many randomly distributed scattering centers, every photon of visible light performs a random walk. Effectively, this random walk slows down light propagation with respect to vacuum and scrambles any incident polarization. Multiple light scattering can also lead to coherent speckles (13) and to Anderson localization (14, 15). For a broad range of settings, however, multiple light scattering is well described by the diffusion of photons (14).

We demonstrate that passive broadband invisibility cloaking of macroscopic objects for all incident directions and polarizations of light is possible in the regime of light diffusion.

In 1855, Fick postulated his diffusion equation (16), which was then followed by a microscopic derivation on the basis of statistical mechanics (17). Our diffusion experiments have been inspired (18, 19) by recent work on thermal cloaking: Whereas early cloaking structures designed with coordinate transformations contained many alternating layers of effectively low and high heat conductivity (20), more recent thermal cloaks (21, 22) work for just one pair of layers with low and high heat conductivity. Such core-shell structures have also successfully been used for static magnetic cloaking (23). Intuitively, the combination of core and shell can be thought of as a single period of a highly anisotropic laminate metamaterial (24). It is known theoretically (24, 25) that core-shell geometries can be perfectly undetectable in the stationary case, assuming a spatially constant gradient of the temperature (or magnetic field or photon density, for example) across the cloak. Recently, it has become clear that these cloaks also work for nonconstant gradients (21, 22). Core-shell geometries allow for cloaks that are thin as compared with the size of the object they hide (21–23).

¹Institute of Applied Physics, Karlsruhe Institute of Technology (KIT), D-76128 Karlsruhe, Germany. ²Deutsche Forschungsgemeinschaft (DFG)–Center for Functional Nanostructures (CFN), KIT, D-76128 Karlsruhe, Germany.

³Institute of Nanotechnology, KIT, D-76021 Karlsruhe, Germany.

*Corresponding author. E-mail: martin.wegener@kit.edu

Fisher information and entanglement of non-Gaussian spin states

Helmut Strobel, Wolfgang Muessel, Daniel Linnemann, Tilman Zibold, David B. Hume, Luca Pezzè, Augusto Smerzi and Markus K. Oberthaler

Science **345** (6195), 424-427.
DOI: 10.1126/science.1250147

Subtle entanglement in an atomic cloud

In the quantum world, atoms can be correlated with each other—"entangled"—which reduces the uncertainty in the knowledge of some of their properties. Physicists then use this reduced uncertainty to perform precision measurements. Strobel *et al.* made an unusual type of entangled state consisting of hundreds of ultracold Rb atoms. These methods may in the future be able to generate states that will be more useful in precision measurement.

Science, this issue p. 424

ARTICLE TOOLS

<http://science.sciencemag.org/content/345/6195/424>

SUPPLEMENTARY MATERIALS

<http://science.sciencemag.org/content/suppl/2014/07/23/345.6195.424.DC1>

REFERENCES

This article cites 34 articles, 3 of which you can access for free
<http://science.sciencemag.org/content/345/6195/424#BIBL>

PERMISSIONS

<http://www.sciencemag.org/help/reprints-and-permissions>

Use of this article is subject to the [Terms of Service](#)

Science (print ISSN 0036-8075; online ISSN 1095-9203) is published by the American Association for the Advancement of Science, 1200 New York Avenue NW, Washington, DC 20005. The title *Science* is a registered trademark of AAAS.

Copyright © 2014, American Association for the Advancement of Science